

Fluorescent Bioprobes: Structural Matching in the Docking Processes of Aggregation-Induced Emission Fluorogens on DNA Surfaces

Yuning Hong,^[a] Hao Xiong,^[a] Jacky Wing Yip Lam,^[a] Matthias Häußler,^[a]
Jianzhao Liu,^[a] Yong Yu,^[a] Yongchun Zhong,^[b] Herman H. Y. Sung,^[a] Ian D. Williams,^[a]
Kam Sing Wong,^[b] and Ben Zhong Tang*^[a, c]

Abstract: Whereas most conventional DNA probes are flat disklike aromatic molecules, we explored the possibility of developing quadruplex sensors with nonplanar conformations, in particular, the propeller-shaped tetraphenylethene (TPE) salts with aggregation-induced emission (AIE) characteristics. 1,1,2,2-Tetrakis[4-(2-triethylammonioethoxy)phenyl]ethene tetrabromide (TPE-1) was found to show a specific affinity to a particular quadruplex structure formed by a human telomeric DNA strand in the presence of K⁺ ions, as

indicated by the enhanced and bathochromically shifted emission of the AIE fluorogen. Steady-state and time-resolved spectral analyses revealed that the specific binding stems from a structural matching between the AIE fluorogen and the DNA strand in the folding process. Computational modeling suggests that the AIE molecule docks

on the grooves of the quadruplex surface with the aid of electrostatic attraction. The binding preference of TPE-1 enables it to serve as a bioprobe for direct monitoring of cation-driven conformational transitions between the quadruplexes of various conformations, a job unachievable by the traditional G-quadruplex biosensors. Methyl thiazolyl tetrazolium (MTT) assays reveal that TPE-1 is cytocompatible, posing no toxicity to living cells.

Keywords: aggregation-induced emission • biosensors • DNA • fluorescent probes • G-quadruplexes

Introduction

Fluorescent biosensors that can selectively identify biologically important macromolecules (e.g., DNA) are powerful analytical tools for studying biological events.^[1] A large variety of fluorescent dyes, such as ethidium bromide, SYBR Green I, and YOYO, have been developed for specific targeting of double-stranded DNA.^[2–4] A single-stranded DNA

rich in guanine (G) base units can adopt a noncanonical structure referred to as a G-quadruplex, a four-stranded structure built from the stacking of several G•G•G•G tetrads and stabilized by cationic species (e.g., K⁺ and Na⁺).^[5] The G-quadruplex structures have attracted much attention in recent decades because of their presence in the genomic regions of particular telomeres and their therapeutic applications as targets for anticancer drugs.^[6,7] The surging interest in the area of G-quadruplex research is calling for the development of specific quadruplex-targeting probe systems.^[8]

Analyses of G-quadruplex structures by X-ray crystallography as well as NMR spectroscopy have revealed a diversity of topological conformations not seen in other DNA systems.^[9] Depending on the length and sequence of a DNA strand, a G-quadruplex structure can be tetra-, bi-, or unimolecular. From the orientation of the strands or the parts of a strand that form G-tetrads, quadruplex structures can be further divided into parallel, antiparallel, and mixed types.^[10,11] Scheme 1a depicts some examples of intramolecular G-quadruplex structures.

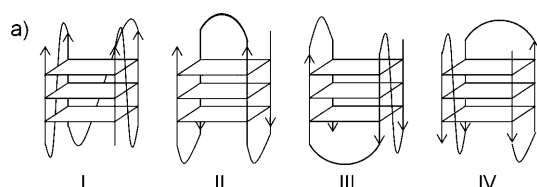
A G-quadruplex offers multiple binding sites. A general strategy for G-quadruplex targeting is to design a probe molecule consisting of a large planar aromatic core prone to

[a] Y. Hong, H. Xiong, Dr. J. W. Y. Lam, Dr. M. Häußler, J. Liu, Y. Yu, Dr. H. H. Y. Sung, Prof. I. D. Williams, Prof. B. Z. Tang
Department of Chemistry, Nano Science and Technology Program
The Hong Kong University of Science & Technology
Clear Water Bay, Kowloon, Hong Kong (P.R. China)
Fax: (+852)23581594
E-mail: tangbenz@ust.hk

[b] Dr. Y. Zhong, Prof. K. S. Wong
Department of Physics
The Hong Kong University of Science & Technology
Clear Water Bay, Kowloon, Hong Kong (P.R. China)

[c] Prof. B. Z. Tang
Department of Polymer Science and Engineering
Zhejiang University, Hangzhou 310027 (China)

Supporting information for this article is available on the WWW under <http://dx.doi.org/10.1002/chem.200900778>.



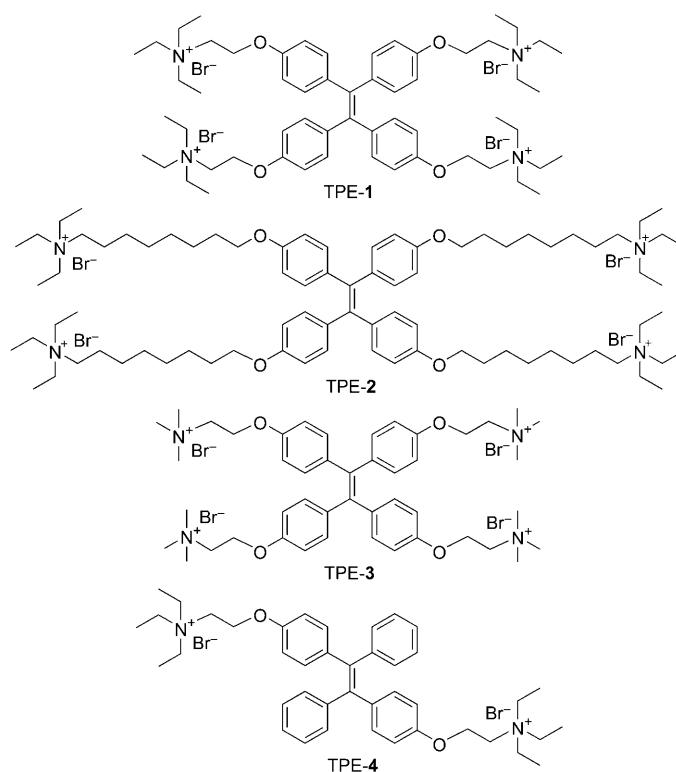
- b) PG12 5'-GGGGGGGGGGGG-3'
 Ap15 5'-GGTTGGTGGTTGG-3'
 Ox28 5'-GGGGTTTTGGGGTTTTGGGG-3'
 CM22 5'-TGAGGGTGGGTAGGGTGGGTAA-3'
 HG21 5'-GGGTTAGGGTTAGGGTTAGGG-3'
 HG22 5'-AGGGTTAGGGTTAGGGTTAGGG-3'
 HG23 5'-GGGTTAGGGTTAGGGTTAGGGT-3'
 HG24 5'-TTAGGGTTAGGGTTAGGGTTAGGG-3'
 HG25 5'-AGGGTTAGGGTTAGGGTTAGGGTAA-3'
 HG26 5'-AAAGGGTTAGGGTTAGGGTTAGGGAA-3'

Scheme 1. a) Representative unimolecular G-quadruplex structures: I) propeller: a parallel structure with three double-chain reversal loops; II) basket: an antiparallel structure with adjacent parallel strands and a diagonal loop; III) hybrid-1: a mixed structure with three parallel and one antiparallel strands; and IV) hybrid-2: a mixed structure with one antiparallel and three parallel strands. b) Abbreviations and sequence of the oligonucleotide strands used in this work.

π - π stacking with the G-tetrad platform and several cationic side arms that facilitate the electrostatic interactions with the anionic DNA strands.^[12] Much effort has been devoted to the search for fluorescent ligands that can differentiate quadruplex from duplex. Through structural tuning, biosensors with high binding affinities to quadruplex over duplex have been successfully developed.^[8,13] The current challenge is to develop new fluorescence probes with specificity for particular individual quadruplex structures amongst the multitude of potential quadruplex-forming sequences.^[14]

Recently, we prepared a water-soluble fluorogen named 1,1,2,2-tetrakis[4-(2-triethylammonioethoxy)phenyl]ethene tetrabromide (TPE-1).^[15] This fluorogen is nonemissive when dissolved but becomes highly emissive when aggregated due to the restriction to its intramolecular rotations by the aggregate formation, thereby showing a novel effect of aggregation-induced emission (AIE).^[16] The AIE behavior is "abnormal" because chromophore aggregation commonly quenches light emission of a fluorophore and decreases its efficiency of DNA detection in the traditional intercalating-type biosensor systems (e.g., cyanine dyes).^[17]

The extraordinary AIE effect of TPE-1 inspired us to utilize it as a DNA probe. In our previous work, we found that in an aqueous buffer, the emission of TPE-1 was turned on when it was docked on the surfaces of DNA folding structures through electrostatic interaction, because the docking process impeded its intramolecular rotations, which in turn blocked the nonradiative channels and populated the radiative relaxations of its excitons.^[15,18] The strong interaction of TPE-1 with DNA enabled rapid visualization of the DNA bands in the poly(acrylamide) gel electrophoresis assays.^[15] The AIE probe discriminated the G-quadruplex structure formed by d[G₃(T₂AG₃)₃] or HG21 (Scheme 1b), a mimic of human telomeric DNA, from the random coil and duplex



structures. The differentiation was signified by a redshift of approximately 20 nm in the emission spectrum of TPE-1, which permitted visual recognition and distinguishability of the G-quadruplex from other DNA structures.^[15]

In this work, we continued our study in this area of research. We systematically designed and synthesized a series of TPE derivatives with different lengths of side arms (TPE-2) and alkyl units of the ammonium groups (TPE-3), and with different numbers of side arms (TPE-4). The TPE derivatives were mixed with the congeners of HG21 with varying sequences (Scheme 1b) in an effort to elucidate the structural effects on the binding of the fluorogens with the G-quadruplexes. Steady-state and time-resolved fluorescence studies revealed a high affinity of TPE-1 to a particular G-quadruplex structure formed by HG21, which is indicative of the involvement of specific structural matching in the binding process. A docking simulation study suggested that the TPE-1 molecule prefers to bind to the grooves on the quadruplex surface with the aid of electrostatic attraction. The specificity of the TPE-1 dye to the HG21/K⁺ quadruplex is utilized to monitor the conformational transformations induced by cationic titrations.

Results and Discussion

Effect of DNA sequence: The oligonucleotides used in this study are all G-rich DNA strands purchased from Invitrogen. PG12 is an oligonucleotide comprising solely of guanine base units (dG₁₂), whereas Ap15 is a thrombin-binding

aptamer with a nucleobase sequence of $d[G_2T_2G_2TG_2T_2G_2]$. Ox28 and CM22 are mimics of the *oxytricha* telomeric repeat ($d[G_4(T_4G_4)_3]$) and the G-quadruplex element in human *c-myc* promoter ($d[TGA(G_3T)_2A-(G_3T)_2A_2]$), respectively. The HG series mimic the human telomeric sequences with a repeat unit of T_2AG_3 . HG26 is similar to that of the wild-type human telomeric sequence and was chosen because of its well-solved, NMR-refined structure in the presence of K^+ .^[19]

The TPE derivatives were synthesized in our laboratories. TPE-1 and TPE-4 were prepared by following our previously published experimental procedures.^[15,20] TPE-2 and TPE-3 were prepared according to the synthetic routes shown in Scheme S1 (in the Supporting Information). All the reaction intermediates and final products were characterized by standard spectroscopic methods, from which satisfactory analysis data were obtained (see the Supporting Information for details).

We first studied photoluminescence (PL) behaviors of TPE-1 in the presence of the G-rich DNA strands and K^+ ions. The buffer solution of TPE-1 gives weak PL signals (Figure 1), which indicate that TPE-1 is soluble in the aque-

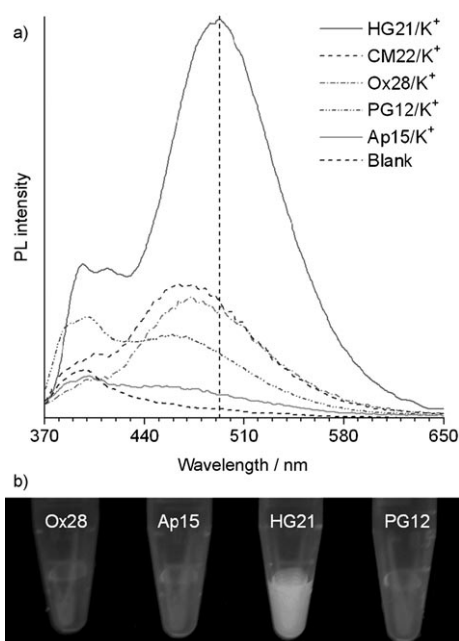


Figure 1. a) Photoluminescence spectra of buffer solutions of TPE-1 in the presence of K^+ ions and G-quadruplexes with different conformations. [TPE-1] = $4.5 \mu\text{M}$, [DNA] = $9 \mu\text{M}$, [K^+] = 0.5M ; λ_{ex} = 350 nm . b) Photographs of TPE-1 solutions in the presence of different G-quadruplexes taken under UV illumination (365 nm).

ous medium. Addition of Ap15, PG12, Ox28, CM22, and HG21 intensifies the PL signals by 2, 5, 7, 10, 12, and 45 times, respectively. The spectrum of the TPE-1/HG21/ K^+ complex shows an emission maximum (λ_{em}) of 492 nm , which is redshifted by approximately 20 nm from those of other DNA systems. Consistently, its excitation maximum

(λ_{ex}) is also observed at a longer wavelength (Supporting Information, Figure S1).

It is known that all the DNA strands are capable of folding into G-quadruplex structures in the presence of K^+ ions but what is the cause for the different fluorescence behaviors of TPE-1? Analysis by circular dichroism (CD) spectroscopy offers some clues. The Ap15/ K^+ complex exhibits positive and negative Cotton effects at 295 nm and 265 nm , respectively, indicative of the formation of an intramolecular antiparallel G-quadruplex structure (Supporting Information, Figure S1). The PG12/ K^+ and CM22/ K^+ complexes give positive CD bands at 265 nm and negative ones at 240 nm , typical of inter- and intramolecular parallel quadruplex structures.^[21] The spectra of HG21/ K^+ and Ox28/ K^+ are similar (positive CD bands at 295 nm with shoulders at 265 nm), which suggests that they take similar conformations in the presence of K^+ ions. The photographs shown in Figure 1b manifest the differences in the interactions of the AIE fluorogen with the quadruplex structures formed by the different G-rich DNA strands. The intense light emission of the TPE-1/HG21/ K^+ complex allows one to differentiate the quadruplex structure formed by the human telomeric sequence from the other quadruplex structures with the naked eye.

Effect of the flanking sequence: The remarkable enhancement in the PL of TPE-1 suggests that the fluorogen has a high binding affinity to the quadruplex structure formed by human telomeric sequences. The orientations of the DNA strands are geometrically governed by the glycosidic conformations of the G units, which determine the morphologies of the G-tetrad cores.^[22] The polymorphism of the G-tetrad cores arising from the different DNA sequences may account for the different association behaviors between the TPE fluorogen and G-quadruplexes. Then what happens if the DNA sequences are assembled into the same G-tetrad structure? The human telomeric sequences (or HG series) with different flanking sequences were thus scrutinized because of their identical G-quadruplex-forming motif. HG21 is a human telomeric sequence without any flanking units at either the 5'- or 3'-end, HG22–HG24 are truncated DNA sequences with either 5'- or 3'-flanking units, and HG25 and HG26 are capped with both 5'- and 3'-flanking units.

Among the AIE fluorogen/G-quadruplex complexes, the TPE-1/HG21/ K^+ system displays the largest emission enhancement and bathochromic shift (Figure 2a). The changes in the λ_{em} value and PL intensity against the HG sequences are plotted in Figure 2b. The emission spectrum of TPE-1/HG22/ K^+ peaks at 455 nm , which is blueshifted approximately 40 nm from that of TPE-1/HG21/ K^+ . The λ_{em} values of the TPE complexes with HG23/ K^+ –HG26/ K^+ are approximately 460 – 470 nm , which is identical to those in the absence of K^+ ions. None of these complexes show emissions stronger than that of TPE-1/HG21/ K^+ .

The CD spectra of HG21/ K^+ –HG26/ K^+ show analogous patterns, which suggests that all of them adopt a similar G-quadruplex topology with indistinguishable strand orienta-

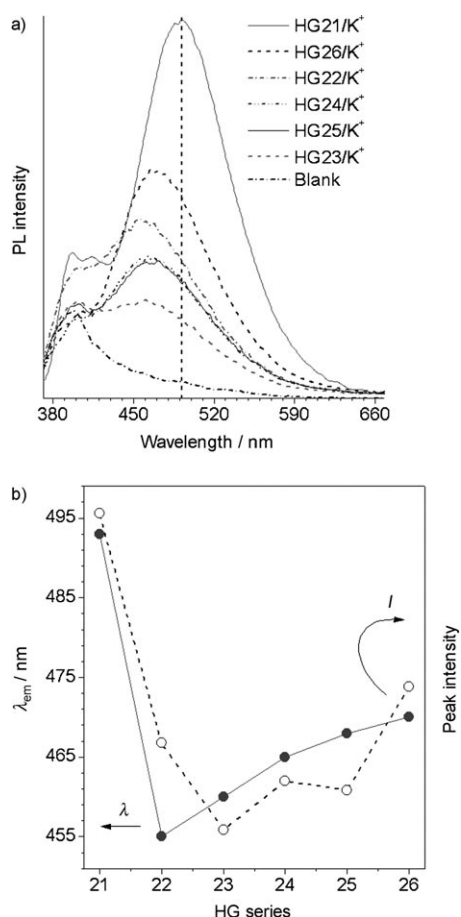


Figure 2. a) Photoluminescence spectra of TPE-1/HG complexes in the presence of K⁺ ions in Tris-HCl buffer solutions. b) Changes in the emission maximum (λ_{em}) and peak intensity of TPE-1 with the variations in the sequences of the HG DNA strands. [TPE-1] = 4.5 μ M, [DNA] = 9 μ M, [K⁺] = 0.5 M; λ_{ex} = 350 nm.

tion and G-tetrad conformation (Supporting Information, Figure S2). The flanking sequences at the 5'- and/or 3'-ends of the DNA strands are critical for accommodation of the loops, which lead to distinct groove dimensions.^[22] The different PL profiles of TPE-1 in the presence of HG21/K⁺ suggest that the loop/groove on the G-quadruplex periphery, rather than the G-tetrad core, plays an important role in the accommodation of the AIE fluorogen.

Effect of cationic species: It is known that cationic species play an important role in determining the structures of G-quadruplexes.^[23] K⁺ and Na⁺ ions can promote the formation of different quadruplex structures from DNA strands with same G-rich sequences. Whereas the HG21/K⁺ complex induces the TPE fluorogen to emit strongly at 492 nm, faint PL is detected in the HG21/Na⁺ system (Supporting Information, Figure S3a). The PL intensity is similar to the isolated species of TPE-1, which indicates that almost no fluorogenic molecules have bound to the HG21/Na⁺ complex. The Na⁺ ions in the buffer solution compete with the

cationic TPE-1 molecule, which hampers its binding to the G-quadruplex and hence weakens its emission.

Evidently, TPE-1 interacts strongly with HG21/K⁺ but weakly with HG21/Na⁺, showing a binding specificity to the K⁺-induced and -stabilized quadruplex of HG21. In other words, TPE-1 has a strong affinity to a specific secondary folding structure of the DNA, rather than its primary strand sequence. Clearly, structure matching between HG21/K⁺ and TPE-1 is the cause for the strong binding preference and unique fluorescence behavior. Although HG26 can assume different G-quadruplex structures in the K⁺ and Na⁺ buffers, the PL spectra of the complexes with TPE-1 are similar in profile (curve shape and peak position), which is suggestive of similar binding behaviors (Supporting Information, Figure S3).

Cation-driven conformational switching: By taking advantage of the spectral differentiation between the K⁺- and Na⁺-driven quadruplex formation, we explored the possibility of modulating DNA folding structures through cationic titration. Addition of a small amount of Na⁺ ions (0.1 M) does not completely quench the emission of TPE-1/HG21 at approximately 470 nm. Figure 3a shows the spectral change of

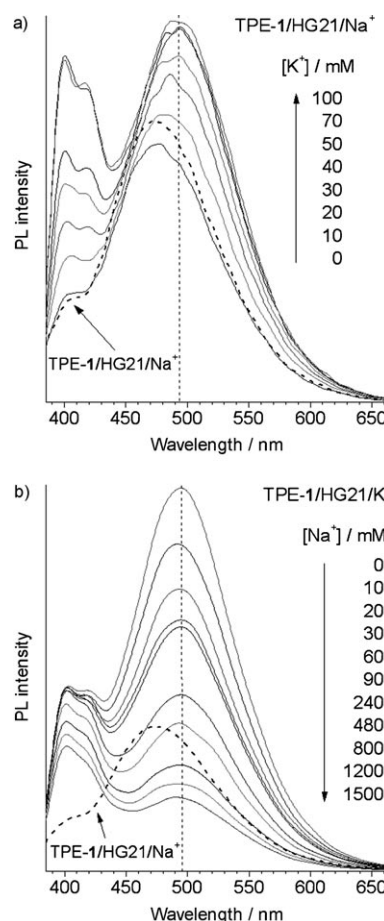


Figure 3. Changes in the emission spectra of buffer solutions of a) TPE-1/HG21/Na⁺ ([Na⁺] = 0.1 M) and b) TPE-1/HG21/K⁺ ([K⁺] = 0.1 M) upon titrations with a) K⁺ and b) Na⁺ ions. [TPE-1] = 4.5 μ M, [HG21] = 4.5 μ M; λ_{ex} = 350 nm.

TPE-1/HG21/Na⁺ with K⁺ titration. The λ_{em} value progressively shifts to the longer wavelength region, accompanied with an increase in the emission intensity. Similar to the main peak, the shoulder at approximately 400 nm is also enhanced and evolves into new peaks in the shorter wavelength region.

The peaks in the short-wavelength region may arise from the TPE molecules bound to the quadruplex through one or two ammonium chelating units. These AIE fluorogens can undergo partial intramolecular rotations. Their twisted conformations decrease the extent of the electronic conjugation, leading to the blueshifted emission. Because of the poor affinity of TPE-1 to HG21/Na⁺, most of the AIE molecules may drift in the buffer solution and experience little interaction with the G-quadruplex. Upon addition of K⁺ ions, the Na⁺-driven quadruplex may gradually alter its conformation to the K⁺-driven one, which attracts the TPE-1 molecule to dock on its surface. After all the best binding sites are occupied, the excess TPE-1 molecules may bind to the G-quadruplex structure through a partial docking mode. The competition between the sodium and ammonium ions may force some of the bound TPE-1 molecules to release one or two ammonium groups from the binding sites. Both of these two events give rise to an increased blue emission at about 400 nm. The negative Cotton effect at 265 nm in the CD spectrum of TPE-1/HG21/Na⁺ is weakened upon addition of K⁺ and its sign is inverted at the high K⁺ concentrations, which is indicative of a conformational transition from the basket structure of HG21/Na⁺ to the mixed structure of HG21/K⁺ (Supporting Information, Figure S4a).

In our previous work, we have demonstrated that TPE-1 can be used as a fluorescence probe to monitor the conformational change of HG21/Na⁺ upon addition of K⁺ ions. What will occur if the K⁺-stabilized quadruplex is titrated with Na⁺ ions? As shown in Figure 3b, addition of Na⁺ ions into the buffer solution of TPE-1/HG21/K⁺ steadily decreases the PL intensity. The Na⁺ ions drive the TPE-1 molecules chemisorbed on the quadruplex surfaces into the aqueous buffer, leading to the observed PL attenuation. The spectral profile, however, remains unchanged even at very high Na⁺ concentrations, suggesting that despite the existence of large excess amount of Na⁺ ions in the buffer solution, the HG21/K⁺ quadruplex maintains its structural integrity.

The G-quadruplex structure formed in the presence of K⁺ ions is undisturbed by the perturbation from the externally added Na⁺ ions, as evidenced by the little variation in the CD spectrum of the HG21/K⁺ complex (Supporting Information, Figure S4b). The K⁺ ions preferentially stabilize the G-quadruplex with folding structures different from those formed in the presence of Na⁺ ions.^[24] Only a low concentration of K⁺ ions is required for the structural stabilization. It is difficult for the Na⁺ ions to reverse the K⁺-stabilized G-quadruplex structure due to their relatively weak induction power. These results indicate that the TPE-1 fluorogen can readily reveal its transition through the change in its PL signal, thus offering a convenient tool for monitoring the

conformational transitions between different quadruplex structures. Further study of the binding modes and mechanisms may help in the understanding of the kinetic processes and folding pathways.

Effect of fluorogen structure: The above results suggest that the unique green emission of TPE-1 arises from a specific topology of the HG21 strand in the presence of K⁺ ions. Alternation in the HG sequences dramatically affects the emission in the longer wavelength region, indicative of geometric structure matching in the binding process of TPE-1 with the quadruplex. To examine whether the molecular structure of the AIE fluorogen is also crucial in the binding event, we prepared a series of TPE derivatives with systematically varied molecular structures.

Derivative TPE-2 contains longer alkyl chains in its side arms than TPE-1. Unlike TPE-1, the dilute buffer solution of TPE-2 shows a relatively strong PL at 475 nm (Figure 4b). The PL is boosted by the addition of HG21. TPE-2 contains a larger hydrophobic unit and its molecules may form micellar aggregates in the aqueous buffer, thereby emitting strongly upon photoexcitation. When bound to the DNA strands, its intramolecular rotations are largely restricted, thus leading to more efficient emission. Interestingly, upon addition of K⁺ ions, its PL is weakened. TPE-2 may become better dissolved in the solution containing K⁺ ions and the disaggregation gives rise to the decrease in the PL of the AIE fluorogen.^[25]

Evidently, the alkyl chain lengths in the side arms of the AIE fluorogen are important in its binding process to the G-quadruplex. How about the ammonium chelating units? To answer this question, we replaced the triethylammonium groups in TPE-1 with less bulky trimethylammonium groups in TPE-3. TPE-3 is even less emissive than TPE-1 in solution but its PL is greatly boosted when HG21 is added. Addition of K⁺ ions weakens the PL of TPE-3/HG21 but brings little change to its spectral profile (Figure 4c). The positively charged ammonium groups in TPE-3 are less sterically shielded, which increases the solubility of the fluorogen in the aqueous buffer and strengthens its interaction with the negatively charged HG21 strand. When the K⁺ ions induce the DNA strand to fold into a G-quadruplex structure, the TPE molecule is detached and driven into the aqueous buffer, probably due to its unfavorable docking on the G-quadruplex surface. The detachment results in the observed PL quenching. Thus, besides the arm length, the molecular structure of the ammonium unit also plays a critical role in the accommodation of the AIE fluorogen by the G-quadruplex.

TPE-4 has only two positively charged side arms. Its solution shows a dim PL, which is only slightly increased by DNA addition (Figure 4d). Due to its lower density of positive charges, TPE-4 has a lower affinity to DNA strands and thus it is difficult for it to emit efficiently in the presence of HG21. TPE-4 has the same, but fewer side arms than its congener TPE-1. It does not show the quadruplex-specific wavelength when it is complexed with HG21/K⁺, similar to

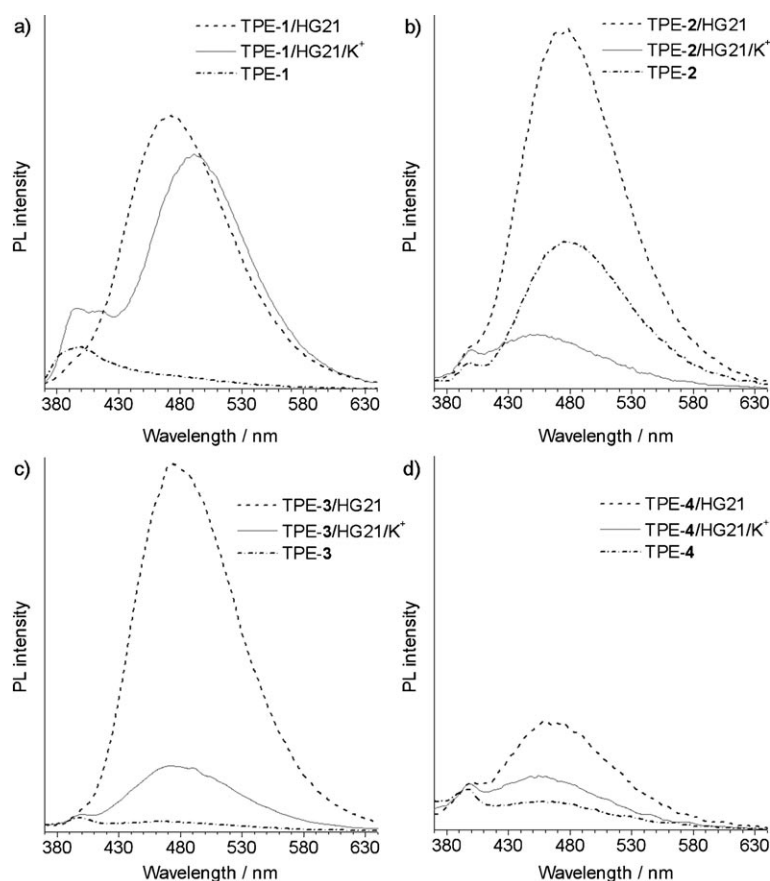


Figure 4. Photoluminescence spectra of HG21 complexes with a) TPE-1,^[15] b) TPE-2, c) TPE-3, and d) TPE-4 in the presence and absence of K⁺ ions. [TPE] = 4.5 μM; [DNA] = 9 μM; [K⁺] = 0.5 M; λ_{ex} = 350 nm.

what was observed in the systems of TPE-2 and TPE-3. These results indicate that the TPE-1 fluorogen possesses the “right” structure for the G-quadruplex recognition.

Time-resolved fluorescence: Time-resolved PL spectra can offer valuable information that is lost during the time-averaging processes of the steady-state spectra measurements. To collect information on the interactions of the fluorogens in the excited states with the environment, their fluorescence lifetimes (τ) were measured. The PL decay traces as well as their fitting curves are shown in Figures S6–S9 (Supporting Information), from which the dynamic parameters were obtained and are summarized in Table 1.

In the absence of DNA, TPE-1 in the aqueous buffer decays in a single-exponential way with a lifetime of 20 ps, which is nearly the resolution limit of the streak camera system (Table 1, entry 1). It is known that τ can be expressed as $1/\tau = 1/\tau_r + 1/\tau_{nr}$, in which τ_r and τ_{nr} denote the radiative and nonradiative lifetimes, respectively. Here τ_r is the intrinsic property of the fluorogen and hence a constant. The short lifetime and low PL efficiency of TPE-1 in the buffer solution suggests that an efficient nonradiative process is involved in the relaxation of the excited states. It is well known that vibrational and torsional motions can non-radiatively deactivate the excited states. In the buffer solu-

tion, the intramolecular rotations of the aryl rings around the axes of the single bonds linked to the central double bond are active, which leads to rapid annihilation of the TPE excitons.

The fluorescence lifetime is lengthened to nanoseconds when the DNA is added to the solution. The PL decay curve is now better fitted by a double-exponential function than the single-exponential one. This indicates that the TPE molecules are now in two different environments, with A_i denoting the fraction of the molecules in each environment. As shown in Table 1, entry 2, upon addition of HG21, 59% of the fluorogen molecules decay slowly with a lifetime of 2.30 ns, which is >100-fold longer than that in the solution without DNA. The remaining 41% of the excited fluorogen molecules decay in a fast mode. The similar behaviors are observed when Ap15/K⁺ and PG12/K⁺ are added

Table 1. Fluorescence decay parameters of dye/DNA complexes.

Entry	DNA/M ⁺ [a]	Dye ^[a]	A ₁ ^[b]	A ₂ ^[b]	τ ₁ [ns] ^[b]	τ ₂ [ns] ^[b]	<τ> [ns] ^[c]
1	–	TPE-1	1	–	0.02	–	0.02
2	HG21	TPE-1	0.41	0.59	0.42	2.30	1.52
3	Ap15/K ⁺	TPE-1	0.65	0.35	0.02	1.19	0.43
4	PG12/K ⁺	TPE-1	0.63	0.37	0.11	4.20	1.62
5	Ox28/K ⁺	TPE-1	0.33	0.67	0.02	1.57	1.06
6	CM22/K ⁺	TPE-1	0.21	0.79	0.02	1.71	1.35
7	HG21/K ⁺	TPE-1	0.25	0.75	0.32	4.23	3.26
8	HG22/K ⁺	TPE-1	0.37	0.63	0.19	2.21	1.46
9	HG23/K ⁺	TPE-1	0.55	0.45	0.13	2.47	1.18
10	HG24/K ⁺	TPE-1	0.28	0.72	0.02	1.86	1.35
11	HG25/K ⁺	TPE-1	0.40	0.60	0.02	3.32	1.99
12	HG26/K ⁺	TPE-1	0.35	0.65	0.17	2.41	1.63
13	HG21/Na ⁺	TPE-1	0.73	0.27	0.02	1.97	0.55
14	HG26/Na ⁺	TPE-1	0.43	0.57	0.23	2.75	1.68
15	HG21/K ⁺	TPE-2	0.59	0.41	0.08	1.75	0.76
16	HG21/K ⁺	TPE-3	0.79	0.21	0.13	2.44	0.62
17	HG21/K ⁺	TPE-4	0.26	0.74	0.24	1.81	1.40

[a] [TPE] = 4.5 μM; [DNA] = 9 μM; [M⁺] = 0.5 M (M⁺ = K⁺, Na⁺). [b] Determined from Equation (8), in which A and τ are the fractional amount and fluorescence lifetime of shorter- (1) and longer- (2) lived species, respectively. [c] Weighted mean lifetime determined from Equation (9).

into the TPE-1 solution (entries 3 and 4). In the systems of Ox28/K⁺ and CM22/K⁺, however, the majority of the TPE molecules decay by means of the slow relaxation channel (entries 5 and 6).

To better understand the dynamic processes, we need to interpret the origins of the two components. The fast decay component has a lifetime similar to that in the pure solution (in the absence of DNA). This component represents the fraction of the free fluorogen molecules in the isolated state, which relax nonradiatively and are thus associated with the weak emission. The slow decay component, on the other hand, is assignable to the bound fluorogen molecules. Our previous mechanism investigation has proved that the restriction to the intramolecular rotations of the fluorogen molecules is the main cause for the AIE effect.^[16,20] Upon complexation with DNA, it becomes difficult for the bound molecules to undergo intramolecular rotations. Impeding the molecular motions blocks the nonradiative channel and populates the radiative decay, thereby making the TPE molecules emissive.

The PL maximum of the TPE-1/HG21/K⁺ complex is located at approximately 490 nm. We thus measured its fluorescence lifetimes at this long wavelength. Two components were observed, with lifetimes of 0.32 and 4.23 ns, respectively (Table 1, entry 7). The longer-lived species predominate ($A_2=75\%$), from which an average lifetime of 3.26 ns is obtained. Close examination of the steady-state PL spectrum of TPE-1/HG21/K⁺ reveals that there is a shoulder band at approximately 400 nm (cf. Figure 1). The PL decay at this short wavelength also relaxes in a biexponential mode. By using the same excitation power (2 mW) as in the above measurement, it is found that half of the excited species relax through the slow decay pathway ($\tau_2=5.49$ ns), while another half decays fast with a lifetime of $\tau_1=40$ ps.

In an effort to gain insight into the dynamic process in the TPE-1/HG21/K⁺ system, power-dependent lifetime measurements were carried out. The lifetimes recorded at 400 nm are shortened with increasing excitation power, while those recorded at 490 nm remain practically unchanged (Figure 5). The results for the PL decays are summarized in Table S2 (Supporting Information). All the decays are comprised of two components. Careful analysis of the dynamic parameters reveals that both the fraction and lifetime of the longer-lived species largely decrease with an increase in the excitation power when the decay curves are measured at 400 nm (Table S2, entries 1–5). The lifetimes of the shorter-lived species, however, do not change much with the power variation.

In contrast, neither the fast component nor the slow component shows a power-dependent lifetime when the decay curve is measured at 490 nm (Table S2, entries 6–10). The fraction of the shorter-lived species is slightly increased with increasing excitation power. The λ_{ex} -dependent steady-state PL measurements reveal the same trend as that observed in the PL decay experiments. Thus, continuous scanning by changing the λ_{ex} from 370 to 300 nm progressively intensifies the emission at 400 nm but causes little change in the PL intensity at 490 nm (Supporting Information, Figure S7).

These results are understandable. A G-quadruplex can offer several sites for the fluorogen molecules to bind. Here we define the one at which a TPE-1 molecule can dock with

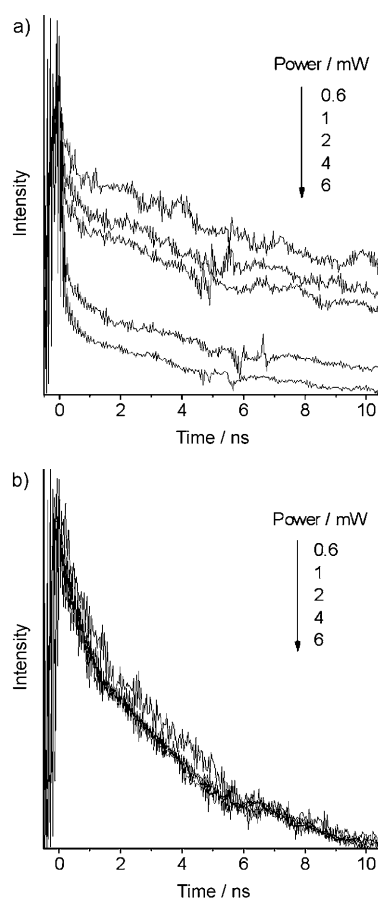


Figure 5. Time-resolved fluorescence decay curves of TPE-1/HG21/K⁺ recorded at a) 400 and b) 490 nm; excitation power was changed in the range of 0.6–6 mW.

the lowest energy as the most favorable binding site. The fluorogen in this locus may contribute to the emission at approximately 490 nm. The unalterable photophysical properties in this region suggest that the best binding sites are all occupied by the fluorogen molecules in this system. Enhancing the excitation power or shortening the λ_{ex} value barely changes the population of the excited species in this state. On the other hand, the emission at the shorter wavelength of approximately 400 nm is from those unbound and/or partially bound molecules. In terms of fluorescence lifetime, these species correlate to the shorter-lived component. Stronger power and/or shorter wavelength can pump more molecules from the ground state to the excited state, thereby increasing the population of the excited species. The amount of the shorter-lived species is thus increased by adjusting the experimental conditions.

To the best of our knowledge, no fluorescence probes have been found that differentiate HG21/K⁺ from HG21/Na⁺ through steady-state PL measurements. Only a small difference in their decay times been observed in time-resolved measurement.^[26] Intriguingly, in terms of lifetime, TPE-1 also behaves differently upon interacting with HG21/K⁺ and HG21/Na⁺. The majority of TPE-1 molecules in the

presence of HG21/Na⁺ relaxes by means of the fast channel, opposite to the case of HG21/K⁺ (Table 1, entry 13). The average lifetime is calculated to be 0.55 ns, which is much shorter than that in the presence of HG21/K⁺ (3.26 ns). The great difference between the two lifetimes offers us with another means to distinguish the two G-quadruplex conformers.

The lifetimes of TPE-2 to TPE-4 complexed with HG21/K⁺ were also measured. All the complexes show shorter lifetimes than TPE-1/HG21/K⁺ does (Table 1, entries 15–17). For TPE-2 and TPE-3, the shorter-lived species dominate the PL decay processes, whereas the relaxation of TPE-4 is mainly by means of the slow pathway. Because of their low binding affinity, most of the TPE-2 and TPE-3 molecules are stripped off from the DNA by the competitive cations and thus undergo the fast PL decay. Since TPE-4 has the same appendage as TPE-1, the fractional amounts of shorter- and longer-lived species are similar (cf. Table 1, entries 7 and 17). This result verifies our hypothesis that structural matching is the key factor that determines the photophysical behavior of TPE-1 in the quadruplex-binding events.

Determination of binding constant: The above experimental data obtained from the steady-state and time-resolved PL measurements suggest that the unusual specificity originate from a geometric fit between TPE-1 and HG21/K⁺. In an effort to understand the complexation process, we evaluated the binding stoichiometry and constant of the TPE-1/HG21/K⁺ complex. We conducted continuous variation analysis by changing the mole fractions of fluorogen and DNA in the buffer solution, with the sum of the fluorogen and DNA concentrations kept constant.^[27]

According to the AIE principle, in the presence of K⁺ ions, only the bound fluorogen molecules emit, whereas the free fluorogen molecules in the buffer solution are practically nonluminescent. The emission intensities of the solutions were recorded and correlated according to a Job plot as shown in Figure 6. The plot has a peak at 0.5, thus giving a 1:1 binding ratio for TPE-1 to HG21 in the presence of K⁺. In the absence of K⁺ ions, however, the TPE-1/HG21 complex is formed in an approximately 3:1 ratio (Supporting Information, Figure S11). The interaction between TPE-1 and HG21 is mainly electrostatic in nature, as proven in our previous publications.^[15,18,20] The K⁺ ions, however, promote HG21 to fold into a G-quadruplex structure, which provides a specific site for the TPE-1 fluorogen to bind or dock.

To obtain the binding constant of TPE-1 to the HG21/K⁺ quadruplex, we conducted a PL titration experiment by adding a solution of HG21 into a solution of TPE-1 with K⁺. The emission was turned on and gradually increased with increasing G-quadruplex concentration, [GQ] (Figure 7a). The binding constant (K_b) for the TPE-1/G-quadruplex complexation can be estimated by analyzing the changes in the PL intensity with the variations in [GQ].^[28] According to the 1:1 ratio obtained from the Job plot, the equilibrium can be represented by Equation (1):

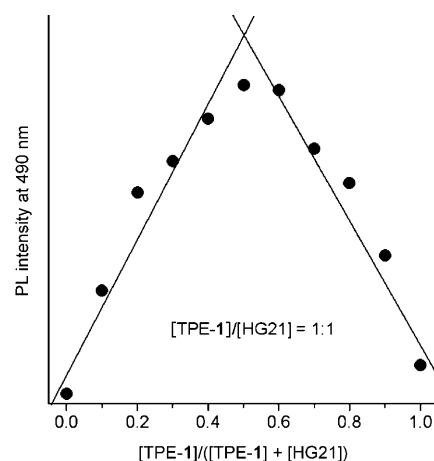


Figure 6. Job plot for determination of the stoichiometry in the binding process of TPE-1 to the G-quadruplex of HG21 formed in the presence of K⁺ ions. The total concentration of TPE-1 and HG21 was kept at 10 μM .

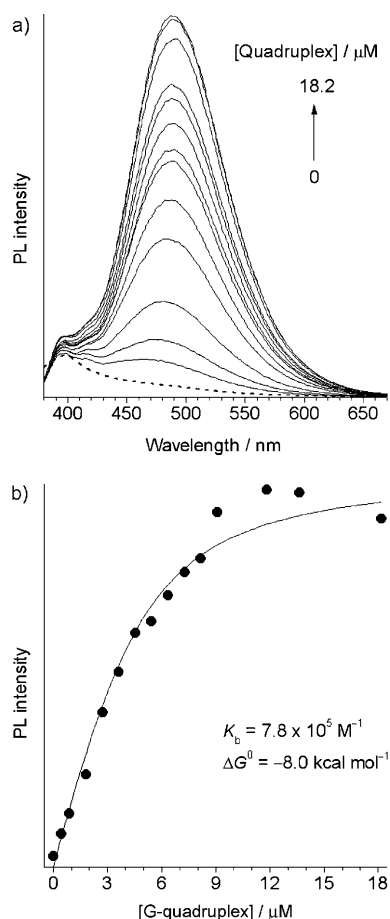


Figure 7. a) Fluorescence titration of HG21 to TPE-1 in the presence of K⁺ ions in 5 mM Tris-HCl buffer. b) Change in the emission intensity at 490 nm with variation in the G-quadruplex concentration and curve fitting using Equation (7). [TPE-1] = 4.5 μM , [K⁺] = 0.15 M; λ_{ex} = 350 nm.



in which GQ denotes the G-quadruplex structure formed by HG21 in the presence of K^+ ions. Because the K^+ concentration is in a large excess amount relative to the HG21 concentration, $[\text{GQ}]$ is equal to $[\text{HG21}]$. K_b for the equilibrium reaction given in Equation (1) can thus be expressed by Equation (2):

$$K_b = \frac{[\text{TPE} - \text{GQ}]_{\text{eq}}}{[\text{TPE}]_{\text{eq}}[\text{GQ}]_{\text{eq}}} \quad (2)$$

in which $[\text{TPE} - \text{GQ}]_{\text{eq}}$ is the equilibrium concentration of the complex for a given G-quadruplex concentration. By using $[\text{TPE}]$ and $[\text{GQ}]$ to denote the total concentrations of the fluorogen and G-quadruplex, respectively, we get Equation (3):

$$K_b = \frac{[\text{TPE}] - [\text{TPE}]_{\text{eq}}}{[\text{TPE}]_{\text{eq}}([\text{GQ}] - [\text{TPE}] + [\text{TPE}]_{\text{eq}})} \quad (3)$$

which can be rearranged to give Equation (4):

$$[\text{TPE}]_{\text{eq}} = \frac{-[K_b([\text{GQ}] - [\text{TPE}]) + 1] + \sqrt{[K_b([\text{GQ}] - [\text{TPE}]) + 1]^2 + 4K_b[\text{TPE}]}}{2K_b} \quad (4)$$

Since PL intensity (I) is proportional to fluorogen concentration, I can thus be considered as a composite of that contributed from the bound and unbound (or free) fluorogen molecules.^[28] The following relationship is therefore established [Eq. (5)]:

$$I = I_{f,\text{max}} \frac{[\text{TPE}]_{\text{eq}}}{[\text{TPE}]} + I_{b,\text{max}} \frac{[\text{TPE} - \text{GQ}]_{\text{eq}}}{[\text{TPE}]} \quad (5)$$

in which $I_{f,\text{max}}$ is the initial, maximum emission intensity of the free fluorogen molecules in the absence of the DNA and $I_{b,\text{max}}$ is the maximum intensity when all the fluorogen molecules are bound to the DNA. On account of their AIE nature, the free TPE molecules are nearly nonfluorescent in the aqueous solution. In other words, $I_{f,\text{max}}$ is negligibly small relative to $I_{b,\text{max}}$. Equation (5) can thus be simplified to give Equation (6):

$$I = I_{b,\text{max}} \frac{[\text{TPE}] - [\text{TPE}]_{\text{eq}}}{[\text{TPE}]} \quad (6)$$

Combining Equations (4) and (6) gives Equation (7):

$$I = I_{b,\text{max}} \left[1 - \frac{K_b[\text{TPE}] - K_b[\text{GQ}] - 1 + \sqrt{(K_b[\text{GQ}] + K_b[\text{TPE}] + 1)^2 - 4K_b^2[\text{GQ}][\text{TPE}]}}{2K_b[\text{TPE}]} \right] \quad (7)$$

In the titration experiment, the fluorogen concentration ($[\text{TPE}]$) is kept constant, while the HG21 concentration

(hence $[\text{GQ}]$) is varied. The K_b value obtained by fitting the titration data with Equation (7) is $(7.8 \pm 0.7) \times 10^5 \text{ M}^{-1}$ for the TPE-1/HG21/ K^+ complex (Figure 7b), from which a Gibbs energy (ΔG°) of $-8.0 \text{ kcal mol}^{-1}$ is obtained from the Gibbs equation.

Thermodynamic parameters: The PL results described above tell us that TPE-1 interacts differently with the HG21/ K^+ and HG21/ Na^+ G-quadruplexes. In an attempt to understand the difference in terms of thermodynamics, isothermal titration calorimetry (ITC) traces were measured. Figure 8a shows the thermograms obtained from the ITC experiment of HG21/ Na^+ with TPE-1 buffer solution. The negative signals indicate an exothermic process. Integration of the area of each injection peak by subtraction of the heat of dilution of TPE-1 furnishes a differential enthalpic binding curve, as shown in Figure 8b.

The isotherm for TPE-1/HG21/ Na^+ titration is virtually identical to that of the dilution of TPE-1 (data not shown), which suggests that there is practically no interaction between TPE-1 and HG21/ Na^+ . The K_b and ΔG° values are determined to be $4.3 \times 10^2 \text{ M}^{-1}$ and $-3.5 \text{ kcal mol}^{-1}$, respectively. Such small values agree well with our earlier findings and indicate a weak binding affinity.^[15] In fact, the small K_b value for TPE-1/HG21/ Na^+ is almost to the detection limit of the apparatus. The titration of TPE-1 into HG21/ K^+ , however, is very different, indicating that TPE-1 molecules interact strongly with HG21/ K^+ (Figure 8b). Nonlinear fitting of the data gives K_b and ΔG° values of $2.4 \times 10^5 \text{ M}^{-1}$ and $-7.3 \text{ kcal mol}^{-1}$, respectively. The data are consistent with those obtained from the fluorescence titration experiment ($K_b = 7.8 \times 10^5 \text{ M}^{-1}$ and $\Delta G^\circ = -8.0 \text{ kcal mol}^{-1}$), which indicates a binding affinity three orders of magnitude higher than that in the TPE-1/HG21/ Na^+ system.

Parallel ITC titration experiments were performed to evaluate the interactions of TPE-1 with HG26/ K^+ and HG26/ Na^+ . As shown in Figure 9a, injections of TPE-1 aliquots into the HG26/ K^+ solution generate exothermic peaks. Integration of the binding isotherms for TPE-1 with HG26/ K^+ and HG26/ Na^+ give similar profiles (Figure 9b): complexation takes place instantly with the injection of the first few aliquots. Further injections cause a progressive merge of the binding isotherm with the dilution curve. This indicates that all the binding sites on the G-quadruplexes are gradually occupied by the TPE-1 molecules and eventually no binding sites are available for accommodation. By fitting the isotherms, the K_b values for the TPE-1/HG26/ K^+ and TPE-1/HG26/ Na^+ complexations are both found to be around $3 \times 10^4 \text{ M}^{-1}$.

The thermodynamic parameters for the fluorogen/G-quadruplex binding processes are summarized in Table 2. In the titration experiment of TPE-1 into the HG21/ K^+ solution, a negative enthalpy change (ΔH°) is involved, which suggests that the

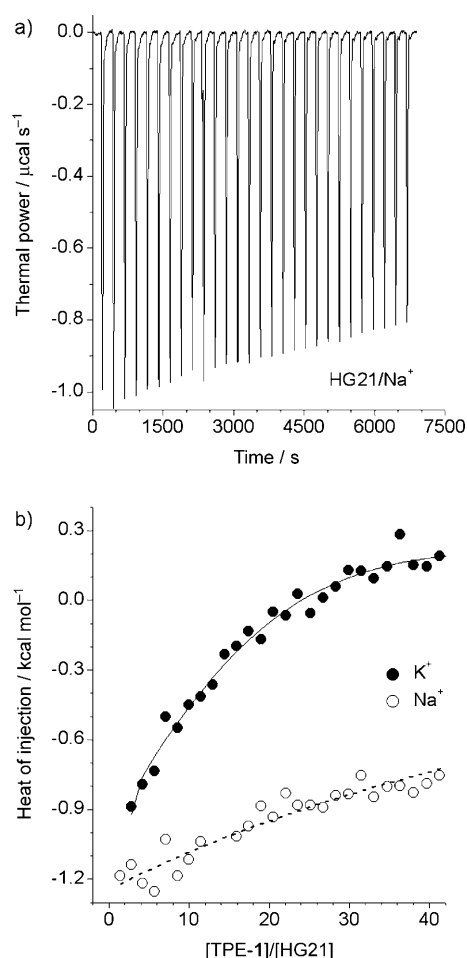


Figure 8. a) Calorimetric curves for titration of HG21 in a Na^+ -Tris buffer with serial injections of TPE-1 at 25°C. b) Binding isotherm as a function of $[\text{TPE-1}]/[\text{HG21}]$ molar ratio in K^+ -Tris^[15] or Na^+ -Tris buffer.

binding is enthalpy-driven. The binding process is further favored by a positive entropy change ($\Delta S^\circ > 0$). This seems surprising but can be understood: it may be caused by the release of the counterions upon electrostatic attraction of TPE-1 to the HG21/ K^+ ensemble. The data resembles those published by other groups, in which the researchers used the ITC technique to determine the binding constants of the cationic ligands to the G-quadruplex.^[27]

The thermodynamic data offer some insights into the driving forces behind the binding process. Various noncovalent interactions such as electrostatic, hydrophobic, and van der Waals forces as well as hydrogen bonding can be involved in a bimolecular complexation process. Judging from the structure of TPE-1, hydrogen bonding can be ruled out. Although hydrophobic interactions are usually characterized by small positive ΔH° and ΔS° values, van der Waals interactions often involve a negative ΔH° value.^[29] The negative ΔH° and positive ΔS° values involved in the formation of TPE-1/HG21/ K^+ complex imply that both hydrophobic and van der Waals interactions are involved in the binding process. Moreover, as revealed by our previous study, electrostatic attractions play an essential role in the fluorogen/G-

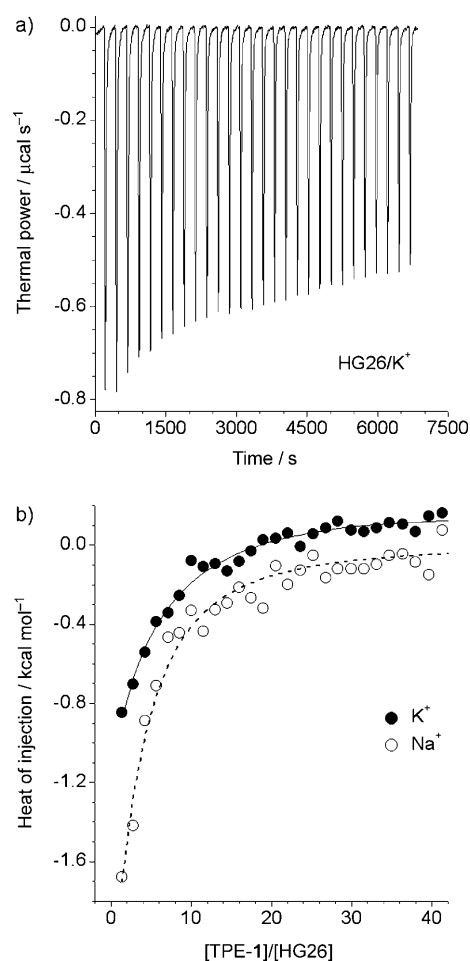


Figure 9. a) Calorimetric curves for titration of HG26 in a Na^+ -Tris buffer with serial injections of TPE-1 at 25°C. b) Binding isotherm as a function of $[\text{TPE-1}]/[\text{HG26}]$ molar ratio in K^+ -Tris or Na^+ -Tris buffer.

Table 2. Thermodynamic parameters for TPE-1 binding with different quadruplexes.^[a]

DNA/ion	K_b [M^{-1}]	ΔH° [kcal mol^{-1}]	ΔG° [kcal mol^{-1}]	$T\Delta S^\circ$ [kcal mol^{-1}]
HG21/ K^+	2.4×10^5	-5.4 ± 0.6	-7.3 ± 0.1	1.9
HG21/ Na^+	4.3×10^2	n.d. ^[b]	-3.5	n.d. ^[b]
HG26/ K^+	3.6×10^4	-1.6 ± 0.3	-6.2 ± 0.1	-0.3
HG26/ Na^+	3.2×10^4	-2.6 ± 0.2	-6.2 ± 0.3	-4.7

[a] Obtained from ITC measurements at 25°C and calculated from Equation (10). [b] n.d.=not determined (binding interaction too weak to be determined accurately).

quadruplex association process.^[15] The binding affinity of TPE-1 to HG21/ Na^+ , on the other hand, is so weak that their thermodynamic parameters are very difficult to determine accurately. Apparently, the topology of the G-quadruplex is vital in the binding event and determines the binding affinity of the fluorogen molecule.

In the titration experiments of TPE-1 with HG26/ K^+ and HG26/ Na^+ , the ΔH° and ΔS° values in both processes are negative, which suggests that the association is enthalpy-driven but entropically unfavorable. Here, the van der

Waals interaction and electrostatic attraction may be the main driving forces for the complexation events. The larger negative ΔH° values arising from the van der Waals interactions compensate for the smaller entropy losses, resulting in the negative ΔG° values in these systems.

Modeling of the binding mode: In an effort to further elucidate the interactions between the fluorogen and quadruplex, we conducted a modeling study. The Autodock software package^[30] was adopted for the computation simulation with the aim of understanding two main issues: how the fluorogen molecule binds to the quadruplex and how the binding interaction alters the photophysical behaviors of the fluorogen. Unfortunately, the folding structure of the HG21/K⁺ G-quadruplex in solution is not available. We thus chose the NMR-refined structure of the HG26/K⁺ G-quadruplex for the docking simulation. The folding structure, which is believed to be similar to that of HG21/K⁺, was retrieved from the protein data bank (PDB) maintained by the Research Collaboratory for Structural Bioinformatics (RCSB).^[19]

In the modeling process, a flexible ligand docking methodology of Autodock^[30] was employed, which allows TPE-1 to enjoy full torsional freedom.^[31] From the 100 configurations generated by the docking simulation, the best binding configuration with the lowest energy was identified (Figure 10a). Distinctly different from the “conventional” end-stacking motif to the G-tetrads, the TPE-1 molecule docks on the surface of the folding structure of the DNA strand. The aromatic core is stacked on the deoxyribose regions of the DNA backbone through carbohydrate- π interactions (gray region).^[32] The ethylene chains are located above the grooves formed by phosphates and sugars, with the alkyl groups of the ammonium groups extruding into the valley between the adjacent phosphate ions (red region). A simplified illustration of the proposed fluorogen/quadruplex binding mode is shown in Figure 11.

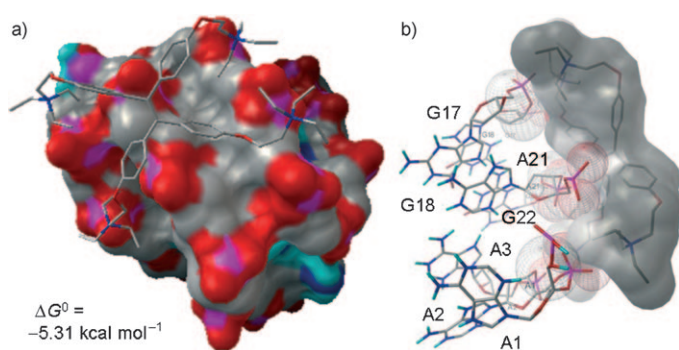


Figure 10. Docking arrangement of TPE-1 on human telomeric G-quadruplex folded by HG26 in the presence of K⁺ (PDB entry of the NMR-refined DNA structure: 2HY9). a) Surface contour depicting the binding locus (TPE-1 shown in sticks). The model is colored for clarity: C in gray, O in red, and P in magenta. b) Stereostructure showing the binding region of the DNA (shown in sticks) for TPE-1 (shown as transparent surface in gray) with labels indicating the residues involved in the binding interaction. Spheres showing the electrostatic potential of the DNA backbone with negative charge in red and neutral in gray.

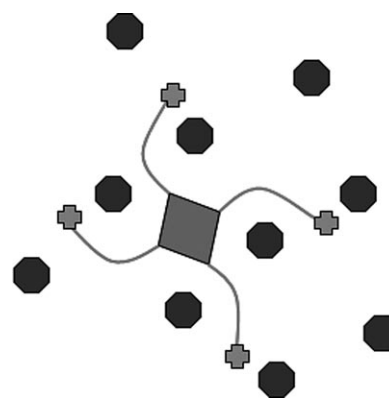


Figure 11. Cartoon illustration of the proposed binding mode. The structure of TPE-1 is simplified as a solid tetragon (tetraphenylethylene core) with four lines (alkyl side arms) and solid crosses (terminal ammonium cations). Phosphates on the DNA backbone are shown as open octagons.

The noncovalent interaction between carbohydrates and aromatic rings has been described as a hydrophobic effect, dispersion force, or C-H \cdots π interaction.^[33] The simulated binding model is in good agreement with our thermodynamic study, which indicates that both the hydrophobic and van der Waals interactions are involved in the binding process. As revealed by the crystalline lattices of the AIE molecules in our previous investigation, the C-H \cdots π interactions can rigidify the conformations of the fluorogen molecules and hamper their intramolecular rotations, thereby making them highly emissive.^[33]

Without exerting any constraints on the C-C single bonds of the TPE core, the phenyl rings have sufficient flexibility to adjust and optimize their conformations. The torsion angles between the aryl planes and the central olefinic double bond determine the λ_{ex} and λ_{em} values.^[22] Through extraction from the docking results, the torsion angle of the fluorogen molecule in the simulated conformation is found to be approximately 51°. The geometry of the HG21/K⁺ quadruplex may differ from that of the HG26/K⁺ quadruplex within the dimensions of the groove. To achieve an optimal binding configuration, the phenyl rings of TPE-1 may have adopted smaller torsion angles, which lead to the observed stronger emission at the longer wavelength in the TPE-1/HG21/K⁺ system.

The positively charged ammonium groups also play an essential role in the binding process. The ammonium units impart good water solubility to the fluorogen molecules and facilitate their approach to the DNA strands. Their electrostatic attractions are critical to the selective binding. The nucleotides involved in the binding region include A1, A2, A3, G17, G18, and G21 (cf. Figure 10b). The negatively charged phosphate units in the DNA backbone assemble perfectly around the positively charged ammonium units with the aid of electrostatic attraction.

Furthermore, the size and shape of the side arms of the AIE fluorogen are part and parcel of the specific recognition. Different from those in the crystalline state, the terminal G-tetrads of the G-quadruplexes are unexposed and

buried by the loops and phosphate backbones in the solution state. The quaternized ammonium groups of the fluorogen may be too bulky to thread through the loop regions and to put the TPE core on top of the G-tetrad. The grooves formed by phosphates and sugars may perfectly accommodate the side arms with spacer lengths of two methylene units. Consistent with the experimental data, changing either the spacer length or the size of the ammonium group results in the disappearance of the characteristic PL features (cf. Figure 4).

The docking models were also simulated on other DNA strands, whose structures could be retrieved from the PDB of RCSB. Table 3 summarizes the binding energies for TPE-

Table 3. Binding energy for TPE-1 to G-quadruplex DNA obtained from the docking simulation.

DNA/ion (PDB entry)	HG26/K ⁺ (2HY9)	HG22/Na ⁺ (143D)	Ap15/K ⁺ (1C32)	CM22/K ⁺ (1XAV)
binding energy [kcal mol ⁻¹]	-5.31	-2.71	-2.16	-1.49

1 to all these quadruplex structures. The docking energy of TPE-1 on the HG26/K⁺ quadruplex is -5.31 kcal mol⁻¹, close to the experimental data (-6.2 kcal mol⁻¹). The binding energies for other G-quadruplexes, however, are much smaller, indicative of unfavorable docking and consistent with the fluorescence results.

Cytotoxicity assay: For a fluorescent bioprobe to be useful practically, it should not interfere with the metabolism of the living system. In other words, it should neither suppress nor stimulate cell-growth process. To examine the biocompatibility of TPE-1, cytotoxicity tests were performed with HeLa cells based on the reduced activity of methyl thiazolyl tetrazolium (MTT).^[34] The HeLa living cells were exposed to different concentrations of TPE-1 buffer solution for 48 h, after which the percentages of the viable cells were quantified. The MTT assay reveals that the cell viability is not significantly altered even when up to 80 μ M TPE-1 is added to the culture medium (Figure 12). Therefore, in addition

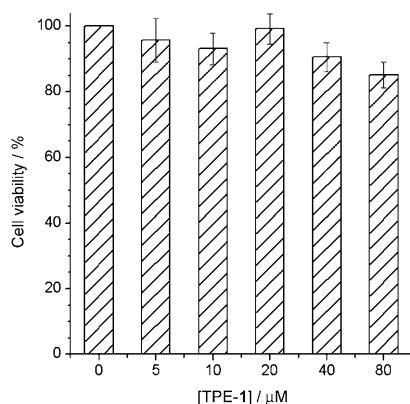


Figure 12. Growth of HeLa cells in the presence of different concentrations of TPE-1 after 2 d incubation.

to the unique quadruplex binding selectivity, cytocompatibility is another merit of the TPE-1 fluorogen system.

The excellent biocompatibility of TPE-1 encouraged us to utilize it for cell staining. The HeLa cells were imaged by TPE-1 using a standard cell-staining protocol. The living cells were incubated with TPE-1 (10 μ M) for 3 h and then washed three times with phosphate buffered saline (PBS) solution. As shown in Figure 13a, the living cells grow

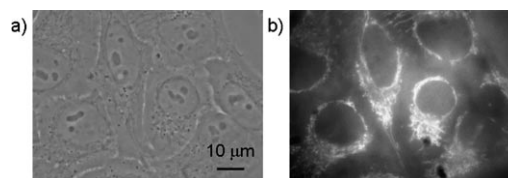


Figure 13. a) Phase contrast and b) fluorescence image of HeLa cells stained with TPE-1. 100 \times magnification; scale bar = 10 μ m; [TPE-1] = 10 μ M.

healthily after being treated with TPE-1. Whereas some commercially available fluorescence dyes, such as CellTracker Green,^[35] stain the entire cells, only the cytoplasmic regions of the cells have been stained by TPE-1, as can be clearly seen from the image taken under UV illumination (Figure 13b). The TPE fluorogen molecules pass through the cell membrane and cluster in the organelles outside the nucleus. The TPE-1 fluorogen may thus be used to probe or monitor biologically important processes in vitro as well as in vivo.

Conclusion

Recent years have witnessed a surge of interest in G-quadruplex studies for diagnostic and therapeutic applications. This calls for the development of highly selective ligands that can specifically bind to the intended target, because of the presence of a large number of G-quadruplex-forming sequences in human genomic DNA and the abundant variations in the G-quadruplex folding structures.

In this work, a series of TPE derivatives with AIE characteristics were synthesized and their potential as G-quadruplex bioprobes was explored. Among the fluorogens, TPE-1 shows excellent selectivity to a particular G-quadruplex structure formed by human telomeric DNA. This specific binding is characterized by a unique redshifted quadruplex emission, offering a convenient visualization method for discriminating not only G-quadruplex from duplex but also between various quadruplex structures. Both experimental and computational results indicate that the specificity arises from a preferred structural matching. With the capability of distinguishing different quadruplex structures adopted by the same DNA sequence under different conditions and by an analogue DNA series with minor differences in the flanking sequences, the TPE-1 fluorogen represents a novel ligand that functions by means of a docking mechanism that

differs from the well-known tetrad-stacking mode. Further studies on the exploration of biomedical applications of the fluorogenic probe are ongoing in our laboratories.

Experimental Section

General information: All oligonucleotides were purchased from Invitrogen (Carlsbad, CA) in desalted quality and used without further purification. Concentrations of the DNA strands were determined by measuring their absorptivity (ϵ) values at 260 nm in a 100 μL quartz cuvette. The ϵ values of the oligonucleotide strands are given in Table S1 (Supporting Information). Water was purified with a Millipore filtration system. The buffer solution was prepared by titrating 5 mM tris(hydroxymethyl)aminomethane (Tris) with 1 N HCl until its pH value reached 7.50. All experiments were performed at room temperature ($\approx 23^\circ\text{C}$) unless specified otherwise. Further experimental details can be found in the Supporting Information.

G-quadruplex formation: Complexes of the oligonucleotides and the TPE derivatives were prepared by mixing a DNA strand (10 μL , 0.1 mM) and a TPE derivative (5 μL , 0.1 mM) in 5 mM Tris-HCl buffer solution in a 1.5 mL Eppendorf cup. The solution was incubated at 4°C for 30 min. G-quadruplex formation was induced by adding a 1.0 M KCl or NaCl solution (10 μL) into the Eppendorf cup. The final concentrations of the TPE derivative and DNA strand were kept at 4.5 and 9.0 μM , respectively.

Lifetime measurement: Fluorescence decay curves were recorded with an Edinburgh Instruments FLS920 combined with steady-state and time-resolved spectrofluorometers. A femtosecond Ti:sapphire oscillator was used as the excitation laser source (200 fs pulse width and 76 MHz repetition rate). The second harmonic (358 nm) of the oscillator output at 716 nm was used for the PL measurement. Time-resolved PL decay curves were measured with a Hamamatsu model C4334 streak camera coupled to a spectrometer. The time resolution was 20 ps. The PL signals were taken at an emission peak of 470 nm, except for the TPE-1/HG21/ K^+ system (490 nm). The laser energy level for excitation is 2 mW. Decay of the fluorescence intensity (I) with time (t) was fitted by a double-exponential function as shown in Equation (8):

$$I = A_1 e^{-t/\tau_1} + A_2 e^{-t/\tau_2} \quad (8)$$

in which τ_1 and τ_2 are the lifetimes of the shorter- and longer-lived species, respectively, and A_1 and A_2 are their respective amplitudes. The weighed mean lifetime ($\langle \tau \rangle$) was calculated according to Equation (9):

$$\langle \tau \rangle = \frac{A_1 \tau_1 + A_2 \tau_2}{A_1 + A_2} \quad (9)$$

Job plot: The continuous variation method of analysis was employed to determine the binding stoichiometry for the TPE-1 and K^+ -driven formation of the G-quadruplex.^[27] The concentrations of TPE-1 and HG21 were varied, while the sum of the two concentrations was kept constant at 10.0 μM . Solutions of TPE-1 and HG21 were prepared in an all-potassium (K^+ -Tris: 5 mM Tris-HCl, 150 mM KCl) aqueous buffer (pH 7.50). In the sample solutions, the mole fraction of the ligand (χ_L) was varied from 0 to 1.0 in 0.1 ratio steps, while the mole fraction of DNA ($1-\chi_L$) was varied accordingly from 1.0 to 0 also in 0.1 ratio steps. Each mixture was incubated at 4°C for 30 min. PL spectra were recorded at 25°C . Fluorescence intensities taken at 490 nm (λ_{em} for the quadruplex-bound TPE-1) were plotted against the mole fraction of the total ligand present. The binding stoichiometry was obtained from the χ intercept (χ_{int} mole fractions of ligand) after linear least-squares fits to the left- and right-hand portions of the Job plot using $\chi_{\text{int}}/(1-\chi_{\text{int}})$.

ITC measurement: The calorimetric titration experiment was performed at $(25.00 \pm 0.01)^\circ\text{C}$ with a MicroCal VP-ITC apparatus. The DNA solutions for the ITC experiments were prepared in all-potassium (K^+ -Tris: 5 mM Tris-HCl and 150 mM KCl) or all-sodium (Na^+ -Tris: 5 mM Tris-HCl

and 150 mM NaCl) buffer at pH 7.50, as required. The buffer solutions of HG21 and HG26 were heated to 85°C and cooled slowly to ensure the folding of the DNA strands into G-quadruplex structures. For a typical titration run, a series of aliquots (10 μL) of TPE-1 solution was injected into the DNA/ M^+ solution at an interval of 240 s. The heat for each injection was determined from the integration of the peak area in the thermogram with respect to time. A blank titration was conducted by injection of TPE-1 solution into the sample cell containing the buffer under identical conditions. The heat of interaction of the TPE-1/HG21 titration was corrected by subtraction of the value from the blank experiment (control). The values of K_b and ΔH° were derived by fitting the isothermal curves by using the Origin 5.0 software.^[36] The ΔG° and ΔS° values were calculated from Equation (10):

$$\Delta G^\circ = -RT \ln K_b = \Delta H^\circ - T\Delta S^\circ \quad (10)$$

Cell culture: HeLa cells were cultured in minimum essential medium containing 10% fetal bovine serum and antibiotics (100 units mL^{-1} penicillin and 100 $\mu\text{g mL}^{-1}$ streptomycin) in a 5% CO_2 humidity incubator at 37°C .

MTT assay: HeLa cells were placed into a 96-well plate at 5×10^3 cells per 0.1 mL per well and treated for 48 h at 37°C with different concentrations of TPE-1 solutions (5, 10, 20, 40, and 80 μM). After the treatment, PBS (20 μL) containing 3-(4,5-dimethylthiazol-2-yl)-2,5-diphenyltetrazolium bromide (MTT; 5 mg mL^{-1}) was added to each well and the plate was incubated at 37°C for 2–4 h. To dissolve intracellular formazan produced by active mitochondria in the living cells, detergent solution (10% w/v sodium dodecyl sulfate in 10 mM HCl; 100 μL per well) was added and the plate was incubated overnight in the dark at room temperature. The absorbance at 595 nm was measured with a spectrophotometric plate reader and used for the calculation of relative cell viability, whereas the cells treated with PBS only were used as the control (100% viability).

Cell imaging: HeLa cells were grown overnight on a plasma-treated 25 mm round cover slip mounted onto a 35 mm Petri dish with an observation window. The living cells were stained with TPE-1 (10 μM) for 3 h. The cells were imaged under an inverted fluorescence microscope (Nikon Eclipse TE2000-U) using a combination of excitation and emission filters: $\lambda_{\text{ex}} = 330\text{--}380$ nm, dichroic mirror = 400 nm. The images of the cells were captured using a computer-controlled SPOT charge-coupled device (CCD) camera (SPOT RT SE 18 Mono).

Computational modeling: The structure of the TPE-1 molecule was optimized with the Gaussian 03^[37] package using the B3LYP method with the 6-31G* basis set. The DNA structure files were retrieved from the RCSB PDB, which include NMR-refined structures of solutions of HG26 with K^+ (2HY9), HG22 with Na^+ (143D), Ap15 with K^+ (1C32), and CM22 with K^+ (1XAV).^[19,38] Docking studies were performed by using the Autodock 4.0^[30] software package in a Core2 Duo 2.4 G CPU Linux terminal.

Acknowledgements

The authors are grateful to the Research Grants Council of Hong Kong (603008 and 602706), the Ministry of Science & Technology of China (2009CB623605), and the National Science Foundation of China (20634020) for financial support. B.Z.T. thanks the support from Cao Guangbiao Foundation of Zhejiang University.

- [1] a) M. W. Pecuh, A. D. Hamilton, *Chem. Rev.* **2000**, *100*, 2479; b) B. N. G. Giepmans, S. R. Adams, M. H. Ellisman, R. Y. Tsien, *Science* **2006**, *312*, 217; c) S. W. Thomas Iii, G. D. Joly, T. M. Swager, *Chem. Rev.* **2007**, *107*, 1339; d) T. L. Halo, J. Appelbaum, E. M. Hobert, D. M. Balkin, A. Schepartz, *J. Am. Chem. Soc.* **2009**, *131*, 438.

- [2] R. Westermeier, N. Barnes, S. Gronau-Czybulka, *Electrophoresis in Practice: A Guide to Theory and Practice*, Wiley-VCH, Weinheim, **1993**.
- [3] a) H. S. Rye, S. Yue, D. E. Wemmer, M. A. Quesada, R. P. Haugland, R. A. Mathies, A. N. Glazer, *Nucleic Acids Res.* **1992**, *20*, 2803; b) A. Fürstenberg, M. D. Julliard, T. G. Deligeorgiev, N. I. Gadjev, A. A. Vasilev, E. Vauthey, *J. Am. Chem. Soc.* **2006**, *128*, 7661.
- [4] a) C. T. Wittwer, M. G. Herrmann, A. A. Moss, R. P. Rasmussen, *BioTechniques* **1997**, *22*, 130; b) G. Cosa, K. S. Focsaneanu, J. R. N. McLean, J. P. McNamee, J. C. Scaiano, *Photochem. Photobiol.* **2001**, *73*, 585.
- [5] a) A. T. Phan, V. Kuryavyi, K. N. Luu, D. J. Patel in *Quadruplex Nucleic Acids* (Eds.: S. Neidle, S. Balasubramanian), RSC, Cambridge, **2006**, p. 81; b) J. L. Huppert, *Chem. Soc. Rev.* **2008**, *37*, 1375.
- [6] a) D. J. Patel, A. T. Phan, V. Kuryavyi, *Nucleic Acids Res.* **2007**, *35*, 7429; b) T. Simonsson, *Biol. Chem.* **2001**, *382*, 621.
- [7] For reviews see: a) J. Fakhoury, G. A. M. Nimmo, C. Autexier, *Anti-Cancer Agents Med. Chem.* **2007**, *7*, 475; b) T. M. Fletcher, *Expert Opin. Ther. Targets* **2005**, *9*, 457; c) S. Neidle, M. A. Read, *Biopolymers* **2000**, *56*, 195.
- [8] a) J. L. Mergny, L. Lacroix, M. P. Teulade-Fichou, C. Hounsou, L. Guittat, M. Hoarau, P. B. Arimondo, J. P. Vigneron, J. M. Lehn, J. F. Riou, T. Garestier, C. Helene, *Proc. Natl. Acad. Sci. USA* **2001**, *98*, 3062; b) M. P. Teulade-Fichou, C. Carrasco, L. Guittat, C. Bailly, P. Alberti, J. L. Mergny, A. David, J. M. Lehn, W. D. Wilson, *J. Am. Chem. Soc.* **2003**, *125*, 4732; c) C. C. Chang, I. C. Kuo, I. F. Ling, C. T. Chen, H. C. Chen, P. J. Lou, J. J. Lin, T. C. Chang, *Anal. Chem.* **2004**, *76*, 4490; d) Z. A. E. Waller, P. S. Shirude, R. Rodriguez, S. Balasubramanian, *Chem. Commun.* **2008**, 1467; e) M. J. B. Moore, C. M. Schultes, J. Cuesta, F. Cuenca, M. Gunaratnam, F. A. Tanious, W. D. Wilson, S. Neidle, *J. Med. Chem.* **2006**, *49*, 582; f) A. C. Bhasikuttan, J. Mohanty, H. Pal, *Angew. Chem.* **2007**, *119*, 9465; *Angew. Chem. Int. Ed.* **2007**, *46*, 9305; g) D. L. Ma, C. M. Che, S. C. Yan, *J. Am. Chem. Soc.* **2008**, *130*, 1835.
- [9] J. Dai, M. Carver, D. Yang, *Biochimie* **2008**, *90*, 1172.
- [10] a) Y. Qin, L. H. Hurlley, *Biochimie* **2008**, *90*, 1149; b) G. N. Parkinson, F. Cuenca, S. Neidle, *J. Mol. Biol.* **2008**, *381*, 1145.
- [11] Webba Da Silva, M., *Chem. Eur. J.* **2007**, *13*, 9738.
- [12] D. Monchaud, M. P. Teulade-Fichou, *Org. Biomol. Chem.* **2008**, *6*, 627.
- [13] E. W. White, F. Tanious, M. A. Ismail, A. P. Reszka, S. Neidle, D. W. Boykin, W. D. Wilson, *Biophys. Chem.* **2007**, *126*, 140.
- [14] a) J. Dash, P. S. Shirude, S. T. D. Hsu, S. Balasubramanian, *J. Am. Chem. Soc.* **2008**, *130*, 15950; b) M. Tera, H. Ishizuka, M. Takagi, M. Saganuma, K. Shinya, K. Nagasawa, *Angew. Chem.* **2008**, *120*, 5639; *Angew. Chem. Int. Ed.* **2008**, *47*, 5557; c) H. Yu, X. Wang, M. Fu, J. Ren, X. Qu, *Nucleic Acids Res.* **2008**, *36*, 5695; d) J. E. Redman, J. M. Granadino-Roldán, J. A. Schouten, S. Ladame, A. P. Reszka, S. Neidle, S. Balasubramanian, *Org. Biomol. Chem.* **2009**, *7*, 76; e) T. Li, E. Wang, S. Dong, *Chem. Eur. J.* **2009**, *15*, 2059; f) J. Elbaz, M. Moshe, B. Shlyahovsky, I. Willner, *Chem. Eur. J.* **2009**, *15*, 3411.
- [15] Y. Hong, M. Haeussler, J. W. Y. Lam, Z. Li, K. K. Sin, Y. Dong, H. Tong, J. Liu, A. Qin, R. Renneberg, B. Z. Tang, *Chem. Eur. J.* **2008**, *14*, 6428.
- [16] For ewviews, see: a) Y. Hong, J. W. Y. Lam, B. Z. Tang, *Chem. Commun.* **2009**, 4332; b) J. Liu, J. W. Y. Lam, B. Z. Tang, *J. Inorg. Organomet. Polym. Mater.* **2009**, *19*, 249.
- [17] A. Fürstenberg, T. G. Deligeorgiev, N. I. Gadjev, A. A. Vasilev, E. Vauthey, *Chem. Eur. J.* **2007**, *13*, 8600.
- [18] a) H. Tong, Y. Hong, Y. Dong, M. Haeussler, J. W. Y. Lam, Z. Li, Z. Guo, Z. Guo, B. Z. Tang, *Chem. Commun.* **2006**, 3705; b) Z. Li, Y. Q. Dong, J. W. Y. Lam, J. Sun, A. Qin, M. Häubler, Y. Dong, H. H. Y. Sung, I. D. Williams, H. S. Kwok, B. Z. Tang, *Adv. Funct. Mater.* **2009**, *19*, 905; c) A. Qin, L. Tang, J. W. Y. Lam, C. K. W. Jim, Y. Yu, H. Zhao, J. Sun, B. Z. Tang, *Adv. Funct. Mater.* **2009**, *19*, 1891; d) Z. Zhao, Z. Wang, P. Lu, C. Y. K. Chan, D. Liu, J. W. Y. Lam, H. H. Y. Sung, I. D. Williams, Y. Ma, B. Z. Tang, *Angew. Chem.* **2009**, *121*, 7744; *Angew. Chem. Int. Ed.* **2009**, *48*, 7608.
- [19] a) J. Dai, C. Punchihiwa, A. Ambrus, D. Chen, R. A. Jones, D. Yang, *Nucleic Acids Res.* **2007**, *35*, 2440; b) J. Dai, M. Carver, C. Punchihiwa, R. A. Jones, D. Yang, *Nucleic Acids Res.* **2007**, *35*, 4927.
- [20] H. Tong, Y. Hong, Y. Dong, M. Haeussler, Z. Li, J. W. Y. Lam, Y. Dong, H. H. Y. Sung, I. D. Williams, B. Z. Tang, *J. Phys. Chem. B* **2007**, *111*, 11817.
- [21] S. Paramasivan, I. Rujan, P. H. Bolton, *Methods* **2007**, *43*, 324.
- [22] a) N. Smargiasso, F. Rosu, W. Hsia, P. Colson, E. S. Baker, M. T. Bowers, E. De Pauw, V. Gabelica, *J. Am. Chem. Soc.* **2008**, *130*, 10208; b) T. I. Gaynutdinov, R. Neumann, I. G. Panyutin, *Nucleic Acids Res.* **2008**, *36*, 4079.
- [23] A. T. Phan, V. Kuryavyi, K. N. Luu, D. J. Patel in *Quadruplex Nucleic Acids* (Eds.: S. Neidle, S. Balasubramanian), RSC, Cambridge, **2006**, p. 100.
- [24] a) R. D. Gray, J. B. Chaires, *Nucleic Acids Res.* **2008**, *36*, 4191; b) A. Ambrus, D. Chen, J. Dai, T. Bialis, R. A. Jones, D. Yang, *Nucleic Acids Res.* **2006**, *34*, 2723; c) C. C. Chang, C. W. Chien, Y. H. Lin, C. C. Kang, T. C. Chang, *Nucleic Acids Res.* **2007**, *35*, 2846.
- [25] M. J. Hollamby, R. Tabor, K. J. Mutch, K. Trickett, J. Eastoe, R. K. Heenan, I. Grillo, *Langmuir* **2008**, *24*, 12235.
- [26] C. C. Chang, J. F. Chu, F. J. Kao, Y. C. Chiu, P. J. Lou, H. C. Chen, T. C. Chang, *Anal. Chem.* **2006**, *78*, 2810.
- [27] H. Han, D. R. Langlely, A. Rangan, L. H. Hurlley, *J. Am. Chem. Soc.* **2001**, *123*, 8902.
- [28] a) J. Mohanty, A. C. Bhasikuttan, W. M. Nau, H. Pal, *J. Phys. Chem. B* **2006**, *110*, 5132; b) M. K. Singh, H. Pal, A. S. R. Koti, A. V. Sapre, *J. Phys. Chem. A* **2004**, *108*, 1465.
- [29] a) M. V. Rekharsky, M. P. Mayhew, R. N. Goldberg, P. D. Ross, Y. Yamashoji, Y. Inoue, *J. Phys. Chem. B* **1997**, *101*, 87; b) P. J. Zheng, C. Wang, X. Hu, K. C. Tam, L. Li, *Macromolecules* **2005**, *38*, 2859.
- [30] G. M. Morris, D. S. Goodsell, R. S. Halliday, R. Huey, W. E. Hart, R. K. Belew, A. J. Olson, *J. Comput. Chem.* **1998**, *19*, 1639.
- [31] K. A. Black, A. G. Leach, M. Y. S. Kalani, K. N. Houk, *J. Am. Chem. Soc.* **2004**, *126*, 9695.
- [32] Z. R. Laughrey, S. E. Kiehna, A. J. Riemen, M. L. Waters, *J. Am. Chem. Soc.* **2008**, *130*, 14625.
- [33] Y. Dong, J. W. Y. Lam, A. Qin, J. Sun, J. Liu, Z. Li, J. Sun, H. H. Y. Sung, I. D. Williams, H. S. Kwok, B. Z. Tang, *Chem. Commun.* **2007**, 3255.
- [34] J. Vrba, P. Dolezel, J. Vicar, M. Modriansky, J. Ulrichová, *Toxicol. in Vitro* **2008**, *22*, 1008.
- [35] Y. Yu, Y. Hong, C. Feng, J. Liu, J. W. Y. Lam, M. Faisal, K. M. Ng, K. Q. Luo, B. Z. Tang, *Sci. China Ser. B* **2009**, *52*, 15.
- [36] T. Wiseman, S. Williston, J. F. Brandts, L. N. Lin, *Anal. Biochem.* **1989**, *179*, 131.
- [37] Gaussian 03, Revision B05, M. J. Frisch, G. W. Trucks, H. B. Schlegel, G. E. Scuseria, M. A. Robb, J. R. Cheeseman, J. A. Montgomery, Jr., T. Vreven, K. N. Kudin, J. C. Burant, J. M. Millam, S. S. Iyengar, J. Tomasi, V. Barone, B. Mennucci, M. Cossi, G. Scalmani, N. Rega, G. A. Petersson, H. Nakatsuji, M. Hada, M. Ehara, K. Toyota, R. Fukuda, J. Hasegawa, M. Ishida, T. Nakajima, Y. Honda, O. Kitao, H. Nakai, M. Klene, X. Li, J. E. Knox, H. P. Hratchian, J. B. Cross, V. Bakken, C. Adamo, J. Jaramillo, R. Gomperts, R. E. Stratmann, O. Yazyev, A. J. Austin, R. Cammi, C. Pomelli, J. W. Ochterski, P. Y. Ayala, K. Morokuma, G. A. Voth, P. Salvador, J. J. Dannenberg, V. G. Zakrzewski, S. Dapprich, A. D. Daniels, M. C. Strain, O. Farkas, D. K. Malick, A. D. Rabuck, K. Raghavachari, J. B. Foresman, J. V. Ortiz, Q. Cui, A. G. Baboul, S. Clifford, J. Cioslowski, B. B. Stefanov, G. Liu, A. Liashenko, P. Piskorz, I. Komaromi, R. L. Martin, D. J. Fox, T. Keith, M. A. Al-Laham, C. Y. Peng, A. Nanayakkara, M. Challacombe, P. M. W. Gill, B. Johnson, W. Chen, M. W. Wong, C. Gonzalez, J. A. Pople, Gaussian, Inc., Wallingford CT, **2004**.
- [38] a) Y. Wang, D. J. Patel, *Structure* **1993**, *1*, 263; b) P. H. Bolton, V. M. Marathias, K. Wang, *Nucleic Acids Res.* **2000**, *28*, 1969; c) A. Ambrus, D. Chen, J. Dai, R. A. Jones, D. Yang, *Biochemistry* **2005**, *44*, 2048.

Received: March 25, 2009

Revised: October 8, 2009

Published online: December 2, 2009